Doping-Induced Temperature Compensation of Thermally Actuated High-Frequency Silicon Micromechanical Resonators

Arash Hajjam, *Student Member, IEEE*, Andrew Logan, and Siavash Pourkamali, *Member, IEEE*

***Abstract*—Temperature compensation of thermally actuated high-frequency single crystalline silicon micromechanical resonant structures via high concentration n-type doping has been demonstrated in this paper. The effect of doping level, structural dimensions, and bias current on temperature coefficient of frequency (TCF) for such resonators has also been investigated. It has been shown that the large negative TCF of the silicon resonators (-38 ppm/°C) can be highly suppressed by doping the devices with a high concentration of phosphorous. The TCF can also be fine tuned by changing the operating bias current of the resonators. Temperature drift characteristics for several high-frequency I-shaped resonators thermally doped under different conditions have been measured and compared. For an ideal doping level, an overall linear temperature drift of −3.6 ppm over the range of 25 °C to 100 °C, which is equivalent to a TCF as low as -50 ppb/°C, has been demonstrated for one of the resonators. The results in this paper imply the possibility of having low-cost high-frequency thermally actuated resonators with a near-zero TCF. [2011-0172]**

***Index Terms*—Degenerate doping, microelectromechanical systems (MEMS) resonator, microresonator, piezoresistive readout, temperature coefficient of frequency (TCF), temperature compensation, temperature drift, thermal actuation.**

I. Introduction

MICROELECTROMECHANICAL silicon resonators are of great interest for miniaturized highly stable frequency generation as well as resonant mass sensing for molecular or particulate detection [1]–[5]. However, relatively large temperature drift of such devices is one of the major drawbacks in their competition against conventional quartz crystals. Silicon resonators typically exhibit temperature coefficient of frequency (TCF) in the -20 to -40 ppm/°C range, which is equivalent to an overall linear temperature drift of ~ -2900 ppm over the range of 25 °C to 100 °C [6], [7], whereas the uncompensated crystal oscillators commercially available have an overall temperature drift of $\sim\pm 20$ to ± 40 ppm over the range of -20 °C to 70 °C [8]. In the meantime, it should be mentioned that temperature-compensated crystal oscillators have an overall temperature drift as low as $\sim\pm 3.5$ ppm over the same temperature range [9].

The relatively large negative TCF of silicon resonators is mainly due to the softening of the structural material as the temperature increases. This change in stiffness translates into a change in the resonant frequency of the structure.

A number of both active and passive temperature compensation techniques have been demonstrated for improvement of the temperature stability of microelectromechanical systems (MEMS) resonators. One of the active temperature compensation approaches is to utilize a tunable resonator along with a temperature-sensitive circuit applying the appropriate tuning signal to the resonator in accordance with changes in temperature [10]. Another active method is to encapsulate the resonator in a miniaturized thermally isolated container (micro-oven). In this approach, heating elements keep the temperature of the isolated area constant at an elevated level to achieve frequency stability [11]–[13]. In addition to the power consumption issues, the general disadvantage of active compensation techniques is the added complexity and cost to the system.

A number of passive resonator temperature compensation techniques, which are generally more desirable, have also been demonstrated. One of such techniques that can only be applied to lower frequency air-gap electrostatic resonators is to make the resonator and its electrode(s) out of different materials. If designed properly, the difference between thermal expansion coefficients of the two materials can tune the gap size and, consequently, the resonator frequency with temperature to cancel out the effect of structural material softening [14]. Another passive temperature compensation technique is utilization of composite structures made of materials with opposing elastic constant temperature dependence [6], [15], [16]. The geometric design of the structure has also shown to contribute to the temperature drift behavior [17]. Finally, high-concentration p-type doping of silicon has proven to be a highly effective and simple temperature compensation solution [18].

Thermally actuated micromechanical resonators have shown the ability to operate at very high frequencies with potentially very low power consumption [19], [20]. Although thermally actuated resonators operate at elevated temperatures due to the bias current required for their operation, they generally follow a similar trend of sharp negative frequency drift as their

Manuscript received June 4, 2011; revised December 8, 2011; accepted January 9, 2012. Date of publication February 22, 2012; date of current version May 28, 2012. Subject Editor C. Nguyen.

A. Hajjam and S. Pourkamali are with the Department of Electrical and Computer Engineering, University of Denver, Denver, CO 80208 USA (e-mail: ahajjam@du.edu; spourkam@du.edu).

A. Logan was with the Department of Electrical and Computer Engineering, University of Denver, Denver, CO 80208 USA. He is now with the University of Southern California, Los Angeles, CA 90089 USA (e-mail: andrew.logan@du.edu).

Color versions of one or more of the figures in this paper are available online at http://ieeexplore.ieee.org.

Digital Object Identifier 10.1109/JMEMS.2012.2185217

1057-7157/$31.00 © 2012 IEEE

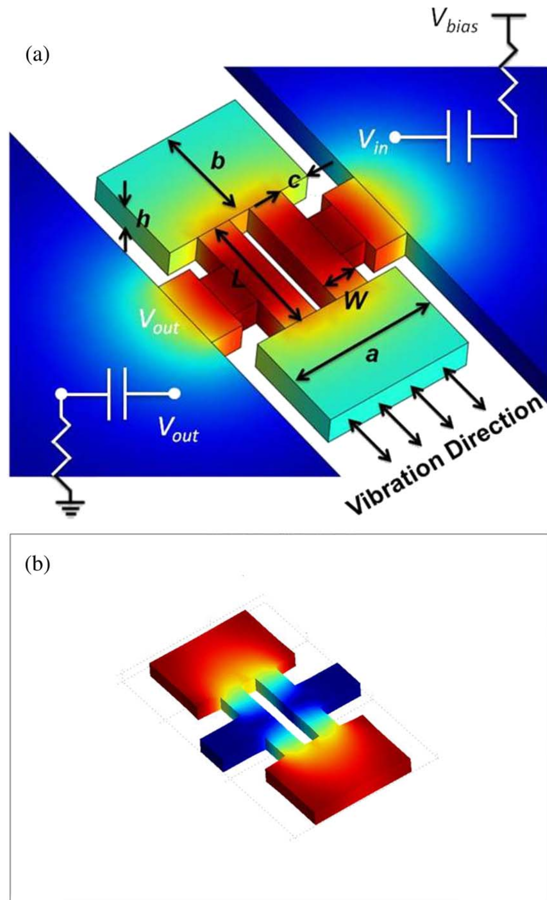

Fig. 1. (a) Schematic of a thermally actuated IBAR showing the qualitative distribution of temperature fluctuation amplitude. The electrical connections required for operation of the resonator are also shown. (b) COMSOL eigenfrequency analysis results showing the fundamental in-plane resonance mode shape for a thermally actuated IBAR. Red and blue colors show locations with the largest and smallest vibration amplitudes, respectively. At resonance, the two plates move back and forth in opposite directions, causing the narrow actuator beams to expand and compress periodically.

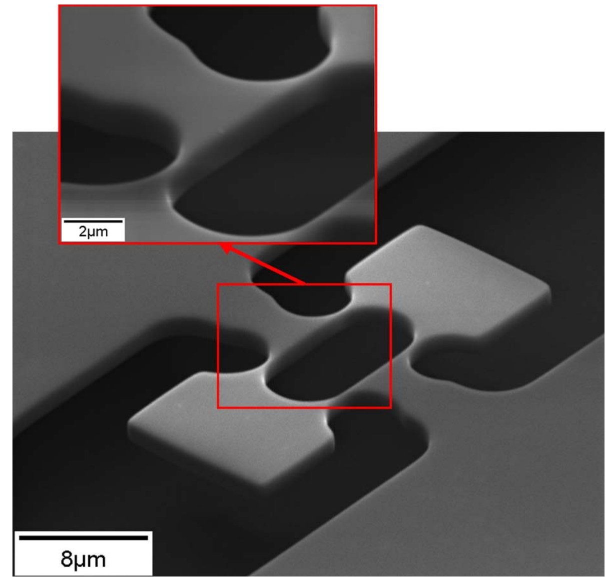

Fig. 2. SEM view of a 60-MHz thermal piezoresistive IBAR and the zoomed-in view of its actuator beams showing their submicrometer width, achieved through thermal oxidation and oxide etch. The resonator is fabricated on a low resistivity (∼0.01 Ω · cm) n-type SOI substrate using a single mask process.

surrounding temperature increases. This is due to the fact that their temperature, even though higher than the surroundings, still changes with the changes in the surrounding temperature. Significantly improved temperature stability has been recently demonstrated for highly n-type (phosphorous) doped single crystalline silicon thermal piezoresistive resonators [21], [22]. In this paper, a more comprehensive study of this temperature compensation technique investigating the effect of different parameters is presented.

II. Resonator Description and Fabrication

The resonators utilized in this work are referred to as I-shaped bulk acoustic resonators (IBARs; also known as dog-bone resonators) [19], [23]. The schematic view of a thermally actuated IBAR is shown in Fig. 1(a).

Such devices are very suitable for thermal actuation and their operating principle has thoroughly been explained in [19]. Actuation occurs by passing a fluctuating electrical current through the actuator beams in the middle of the structure.

Fig. 1(b) shows the in-plane extensional resonant mode of such resonators. In this mode, the masses on the two ends of the beams vibrate back and forth in opposite directions. At resonance, the resistance of the pillars is modulated by the resulting alternating mechanical stress due to the piezoresistive effect. This results in a detectable small signal motional current in the device.

The standard single mask silicon-on-insulator (SOI) MEMS process was used for fabrication of the suspended resonant structures. This process includes carving the single crystalline silicon structures into the SOI device layer using deep reactive ion etching followed by removing the underlying buried oxide (BOX) layer in hydrofluoric acid [19]. The resonators were fabricated on low resistivity n-type SOI substrates with BOX thickness of 5 μm and two different device layer thicknesses of 5 and 10 μm.

Fig. 2 shows the SEM view of a fabricated 60-MHz IBAR. To reduce the bias current required for operation of the resonators and minimize their power consumption, the actuator beams were narrowed down by performing a number of consecutive thermal oxidation and oxide removal steps after the devices were released. At the same time, the resonator thicknesses were also reduced.

The mechanical stiffness of the IBAR structures in the in-plane extensional resonant mode of interest (Fig. 1) is supplied by the actuator beams. Since the IBAR resonators in this work have very narrow actuator beams, high dopant concentration levels can be achieved all the way through the bulk of the beams using relatively short doping and drive-in steps. This highly reduces the amount of time required for doping compared to the bulk structures in [18], making it a much more convenient approach.

III. Measurement Results

Temperature-induced frequency drift of the fabricated resonators were measured by placing them in a temperature controlled oven and monitoring their resonant frequencies at

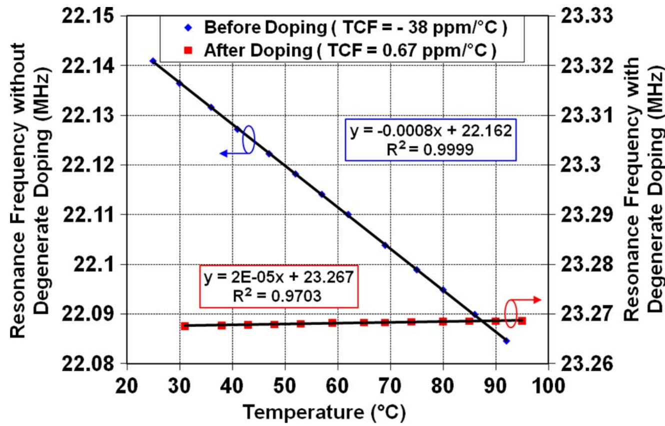

Fig. 3. Measured temperature drift characteristics for two similar IBARs before and after being highly doped with phosphorous. The undoped resonator shows TCF of −38 ppm/°C, while the temperature drift coefficient for the doped resonator has decreased significantly and even turned positive to the value of +0.7 ppm/°C.

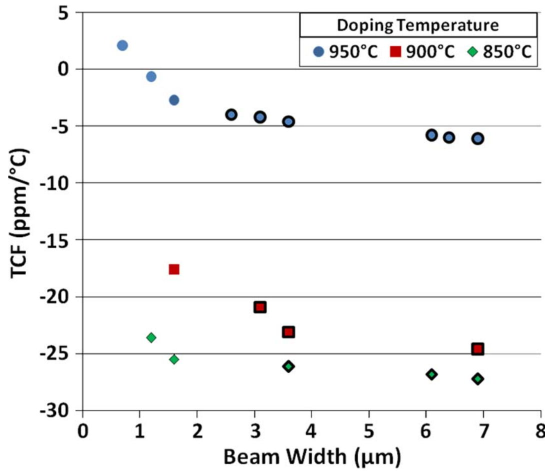

Fig. 4. Measured TCF values for different highly phosphorous doped resonators based on the temperature to which they were doped at and also the maximum width of actuator beams (stiffness element) in the middle of their structure. All the resonators were doped and annealed for a duration of 1 h, respectively. The data points with the black marker line color around them are I^3-BARs for which the width of their central beam was taken into account while the ones without any maker line are I^2-BARs.

different elevated temperatures. The blue plot in Fig. 3 shows the measured frequency drift of −38 ppm/°C for a 22.1-MHz IBAR. It was observed that as expected, the elevated temperature of the resonator due to the current flows does not affect its temperature drift characteristics.

To investigate the effect of doping on such resonators, a similar device was doped at 950 °C for 2 h using a solid phosphorous source followed by 2 h of annealing at 1100 °C (drive-in). The measured temperature drift behavior for this resonator is shown by the red plot in Fig. 3, showing a TCF of +0.7 ppm/°C.

Obtaining a positive value for the temperature drift coefficient of frequency after doping is very interesting. This positive TCF value, which was obtained due to the high dopant concentration penetrating through the narrow beams, shows that if different parameters are optimized, it should be possible to keep the TCF exactly where the transition from negative to positive TCF occurs and, therefore, have a zero TCF point.

TABLE I

MEASURED TCF VALUES AND OTHER CHARACTERISTICS FOR DIFFERENT HIGHLY PHOSPHOROUS DOPED RESONATORS UNDER DIFFERENT BIAS CONDITIONS. THE RESONATORS WERE SIMILARLY PHOSPHORUS DOPED FOR DIFFERENT DURATIONS AND AT DIFFERENT TEMPERATURES AND LATER ANNEALED AT A TEMPERATURE OF 1100 °C FOR 1 h

Resonator Dimensions (µm)						Freq. (MHz)	Q_{air}	Bias DC (mA)	R_{DC} (Ω)	Power (mW)	Doped Temp. (°C)	TCF ppm/°C
a	b	L	W_L	W_m	H							
33	23	36	1.6	-	4.6	21.8	5200	68.9	18.9	89.72	950	**-3.95**
							4400	81.2	18.9	124.6	950	**-2.7**
							4100	88.3	18.9	147.3	950	**-2.1**
33	23	36	1.6	3.6	4.6	28.2	5850	66.6	21.5	95.36	950	**-5.8**
							5200	79.9	21.5	137.2	950	**-4.6**
33	23	36	1.6	6.9	4.6	37.2	3600	67.4	19.1	86.76	950	**-6.3**
							3150	75.5	19.1	108.8	950	**-5.9**
31.4	22.3	36	1.2	-	8.2	18.2	5390	56.5	18.2	58.09	950	**-1.2**
							4800	65	18.2	76.89	950	**-0.65**
30.2	21.8	36	0.7	-	7.8	18.3	5700	45.7	14.1	29.44	950	**2.1**
							5450	59.2	14.4	50.46	950	**2.65**
33	23	36	1.6	3.1	8.2	25.1	3740	56.8	18	58.07	950	**-4.7**
							3400	64.7	18	75.34	950	**-4.2**
33	23	36	0.8	2.6	8.2	24.7	5400	48	14.6	33.63	950	**-4.3**
							5150	61.2	14.6	54.68	950	**-4**
33	23	36	1.6	6.4	8.2	28.6	4270	56.9	17.7	57.30	950	**-6**
							4050	73.6	17.7	95.88	950	**-5.9**
33	23	36	0.7	6.1	8.2	31.4	4700	57.3	14.9	48.92	950	**-6.1**
							4550	67.9	14.9	68.69	950	**-5.8**
33	23	36	1.6	-	4.6	29.1	6500	39.6	97.1	152.2	900	**-21.2**
							6350	46.3	97.1	208.1	900	**-17.6**
33	23	36	1.6	3.6	4.6	31.8	5450	45	103	208.5	900	**-23.1**
33	23	36	1.6	-	4.6	22.8	8100	24.4	116	69.06	850	**-25.5**
33	23	36	1.6	3.6	4.6	33.4	6050	17.4	125	37.84	850	**-26.4**
33	23	36	1.6	6.9	4.6	37.2	5870	12.3	119	18	850	**-27.2**
30.6	20.6	14.9	0.7	-	2.6	23.2	2600	5.31	50.5	1.42	950*	**0.67**
30.2	20.2	30.8	0.2	-	2.2	8.21	7500	1.07	155	0.18	950*	**-0.54**
							7000	1.30	155	0.26	950*	**-0.05**
15	10	11.7	0.8	-	3.5	60.6	490	12.5	46.5	7.29	950*	**-2.4**
						59.2	395	17.1	46.5	13.6	950*	**-1.8**

*: Dope duration was 2 hours instead of 1 hour.

A. *Dependence of TCF on Resonator Beam Width and Doping Temperature*

To investigate the dependence of TCF on doping level, a number of resonators with different stiffness element width were doped at different temperatures.

As can be seen in Fig. 4, for resonators doped at the same temperature, the ones with the narrower actuator beams have a less negative TCF in comparison to those with wider actuator beams. This is due to higher dopant concentration being achievable all the way through the bulk of the beams (stiffness element) for the narrower beams.

Comparison between I^2-BARs (I-shaped resonators with two extensional actuating beams) and I^3-BARs (I-shaped resonators with three extensional beams) generally shows that for the

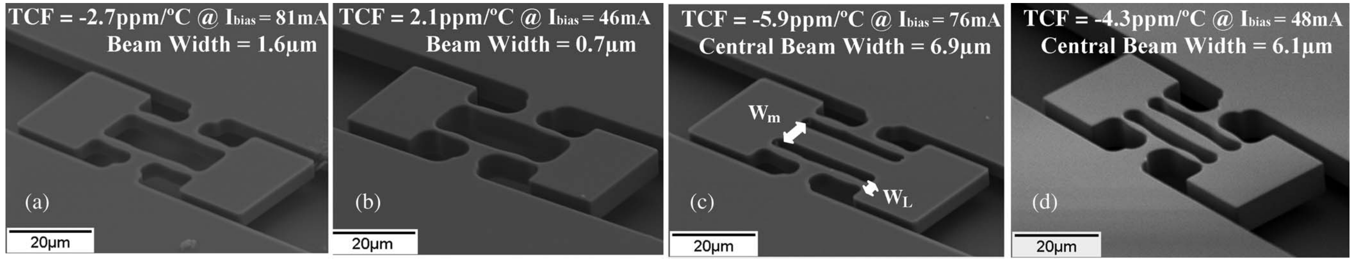

Fig. 5. (a) SEM view of a 21.8-MHz I^2-BAR. (b) SEM view of an 18.3-MHz I^2-BAR fabricated on a similar substrate. This device was initially identical to the previous device, but its actuating beams were narrowed down by thermal oxidation and removal steps. (c) SEM view of a 37.2-MHz I^3-BAR. Dimensions of the two plates and the lateral actuating beams are similar to the I^2-BAR. (d) SEM view of a 24.7-MHz I^3-BAR, which, again, has had its actuating beams narrowed down using thermal oxidation steps. All devices were fabricated on [100] SOI low resistivity n-type substrates and were phosphorus doped for 1 h under similar conditions at a temperature of 950 °C. They were then annealed at a temperature of 1100 °C for an hour.

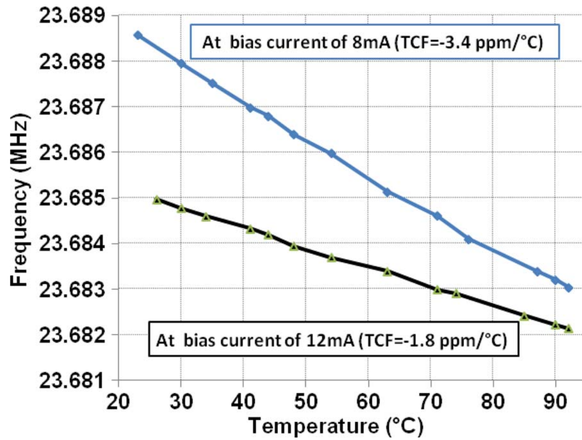

Fig. 6. Temperature drift characteristics for a 23.6-MHz resonator measured under two different bias currents.

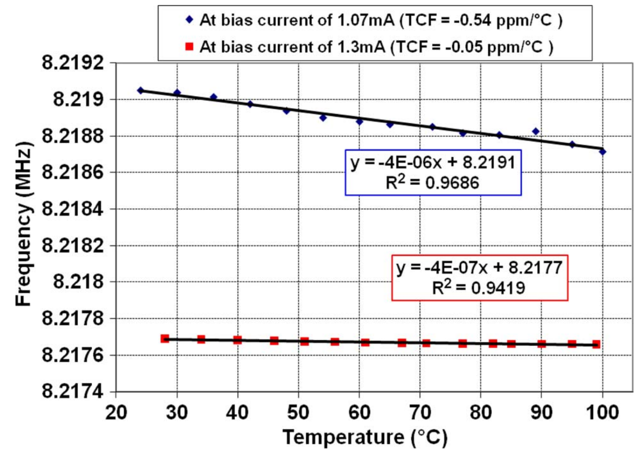

Fig. 7. Temperature drift characteristics for a highly doped 8.2-MHz resonator measured at two different bias currents. Similar to Fig. 6, higher bias current results in a higher TCF (lower negative TCF). By choosing an optimized bias current, a TCF as low as -0.05 ppm/°C has been achieved.

I^3-BAR devices, due to the thicker third beam, which was the beam width shown and taken into account in Fig. 4 (thicker beam = thicker stiffness element), those devices are generally less temperature compensated.

Fig. 4 also demonstrates that, as expected, higher doping temperatures result in higher dopant concentrations, leading to less negative (or more positive) TCF values. It should be mentioned that the doping times above 1 h did not have a noticeable effect on the TCF measurements. In earlier experiments, the resonators were doped for 2 h. It was later realized that only 1 h of doping time was sufficient to get close to zero TCF.

Table I summarizes measured TCF values for a number of different IBAR resonators at different bias currents, some of which are shown in Fig. 5.

It is clearly visible that as the width of the beam gets narrowed and also with an increase in doping temperature, the TCF values tend to become more positive.

B. Dependence of TCF on Bias Current

One interesting trend that can be observed for the doped resonators is that when operated at higher bias currents the TCF values become more positive (or less negative). Fig. 6 shows the measured temperature characteristics of a highly doped 23.6 MHz resonator measured at two different bias currents.

The two plots show slightly different TCF values, showing that the resonator TCF can be tuned by changing its operating bias current. Such tuning capability shows that by having the right doping level and bias current, zero TCF is potentially achievable for such devices.

This is demonstrated in Fig. 7, which shows a similar trend for the measured TCF of a highly doped 8.2-MHz resonator operating at two different bias currents. By adjusting the bias current, a linear temperature drift as low as -0.05 ppm/°C, equivalent to an overall temperature drift of -3.6 ppm over the range of 25 °C to 100 °C, has been achieved for this resonator. At such a high stability level, we are basically limited to our measurement accuracy and the real TCF could even be lower than the mentioned value.

It is also relevant to mention that before temperature compensation, the resonant frequency of thermally actuated resonators is sharply dependent on their bias current. This is due to the fact that any change in bias current translates into a change in the temperature of the device (Joule heating) and, therefore, a frequency drift. This could be a major problem for implementation of frequency references because any noise or fluctuations in the bias current of such devices will turn into oscillator phase noise or change in frequency.

The temperature of a heat source depends on the amount of heat generated as well as the thermal conductance between the source and its surrounding environment. Higher power leads to proportionally higher temperatures; higher thermal conductivity leads to better dissipation of heat and, therefore, a lower temperature at the source. Therefore, to demonstrate the dependence of the resonator frequency on the bias current and its correlation with TCF, a parameter T' has been defined. This is mainly because, due to different device dimensions, a direct comparison of the dependence of the resonator frequencies on their bias current would not be a valid (apple to apple) comparison. This parameter (T') was calculated by dividing the power consumed (P) in the resonator actuator beams by a factor proportional to its thermal conductance (K_{Th}). K_{Th} was determined by dividing the cross-sectional area (A) of the beam by its length (L). The value of T' is proportional but not equal to the actual temperature of the device. Since the changes in T' are proportional to the changes in the temperature difference between the actuating beams of the devices and the surroundings (room temperature), T' is a useful tool to compare the normalized behavior of different parameters in an appropriate manner.

Fig. 8 shows the measured frequency change for different resonators versus T'. The graphs include the normalized frequency shift data (in parts per million) with respect to the frequency measured at the lowest bias current for each of the devices, which have been used as the reference point (set to zero). The resonant frequency change with increased normalized temperature is much higher (7000–8000 ppm range) with increase in the bias current for the less compensated resonators than in the highly doped temperature-compensated resonators, where the overall frequency shift is shown to be much less (less than 200 ppm). Therefore, it can be seen that for doped resonators operating at lower temperatures (lower bias currents), the sharp dependence of resonance frequency on bias current is highly suppressed. It has, however, been observed that for some devices with high operating temperatures, nonlinear/secondary effects such as structural thermal stress could lead to high current dependence of resonant frequency.

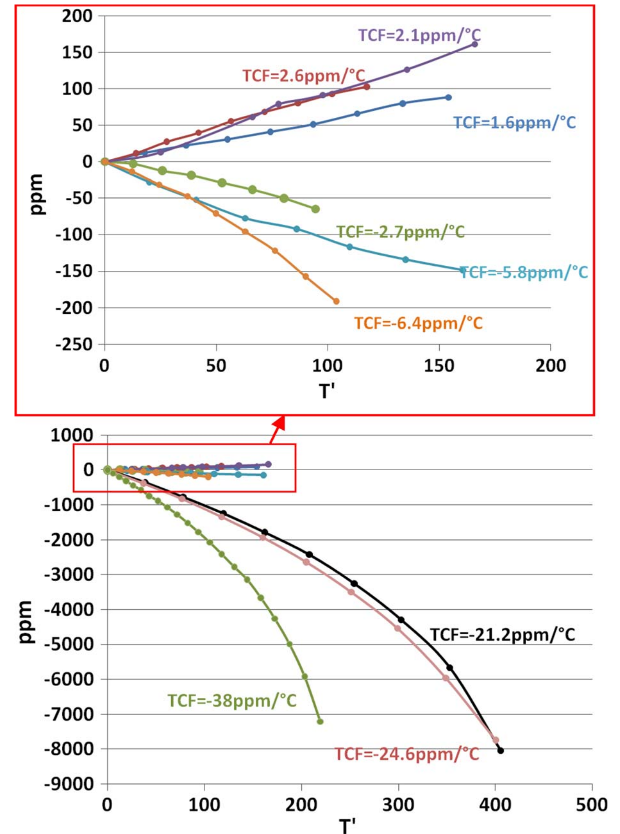

Fig. 8. Dependence of frequency on the normalized temperature of several resonators with different TCF values. For the less compensated resonators, the resonant frequency change is much higher (7000–8000 ppm range) with an increase in the actuating beam normalized temperature, while in the highly doped temperature compensated resonators, the overall frequency shift is shown to be significantly suppressed. Zoomed-in view shows significantly lower frequency shifts (less than 200 ppm) of the highly doped resonators with increase in the temperature of the actuating beams. It should be mentioned that this trend can only be observed for resonators operating at lower temperatures.

IV. Discussion

The exact phenomena leading to doping-induced temperature compensation of micromechanical resonators are not completely understood at this point. One possible justification is the nonlinear dependence of the electronic bandgap of silicon on mechanical strain. It is well known that the electronic bandgap of silicon changes due to mechanical stress and applying tensile stress results in reduction of the gap size [24]. Although to the best of our knowledge no accurate data are available in the literature, most likely, this dependence is not a linear function and includes some higher order terms, i.e., $E_g = E_0 - C_1 \cdot \varepsilon + C_2 \cdot \varepsilon^2 + \ldots$, where ε is the applied tensile strain, E_g is the strain dependent energy level of an electron in the conduction band of silicon, and E_0 is the initial bandgap.

It is known from basic physics that when stored energy level in a system is displacement dependent, mechanical forces are formed tending to move the system toward lower energy levels: $F = -dE/dx$. Based on the same principle, the strain-dependent energy of electrons in the conduction band of silicon $(E_e = nE_g = n(E_0 - C_1 \cdot \varepsilon + C_2 \cdot \varepsilon^2 + \ldots))$ results in an internal mechanical force $(F_{\mathrm{electrical}} = n(-C_1 + C_2.\varepsilon))$. Here, n is the number of carriers in the energy band.

This force has a constant term coming from the linear term in the electronic gap–strain equation and a term that is proportional to the applied strain and comes from the second-order term of the gap equation. This term is equivalent to a mechanical stiffness that can be referred to as the electrical stiffness $(K_{\mathrm{electrical}})$ because it is a result of the electrical energy level in the system. If the electrical stiffness is a function of temperature, which increases with temperature $K_{\mathrm{electrical}} = n \cdot C_2(T)$, it can compensate the effect of mechanical stiffness shrinking with temperature.

Since the temperature coefficient of the electrical stiffness increases by increasing the number of electrons, at high doping levels, its value could become large enough to compensate and even supersede the effect of the temperature coefficient of the mechanical stiffness. Furthermore, since the number of free carriers increases with temperature, the effect of this electrical stiffness increases as the resonator is operated at higher bias currents.

Another possible justification for the change in the TCF with bias current could be the stress induced in the structure due to the changes in its temperature balance as the bias current changes. When the bias current increases, the narrow actuating beams heat up more in comparison to the plates that dissipate more heat through convection. This causes an internal stress in the structure and possibly a change in the TCF [17].

V. Conclusion

Doping-induced temperature compensation of thermally actuated n-type single-crystal silicon micromechanical resonators was demonstrated. Measurement data showing the correlation between doping concentration throughout the resonator stiffness elements and resonator TCF were presented, showing that, as expected, higher doping concentrations lead to a less negative (more positive) TCF.

While highly suppressed temperature drifts were achieved for highly doped structures, it was observed that the resonator bias current provides an added degree of freedom, enabling further fine tuning of the resonator TCF. Temperature-compensated resonators with fine-tuned overall temperature drifts as low as -3.6 ppm over the range of 25 °C to 100 °C were demonstrated.

Temperature compensation using the presented technique can not only minimize the temperature drift, but also is expected to improve the short-term stability, including phase noise characteristics of oscillators implemented utilizing such frequency references by eliminating the sharp dependence to electronic noise in the resonator bias current.

References

[1] R. Abdolvand, H. Mirilavasani, G. K. Ho, and F. Ayazi, "Thin-film piezoelectric-on-silicon resonators for high-frequency reference oscillator applications," *IEEE Trans. Ultrason., Ferroelectr., Freq. Control*, vol. 55, no. 12, pp. 2596–2606, Dec. 2008.

[2] C. T.-C. Nguyen, "MEMS technology for timing and frequency control," *IEEE Trans. Ultrason., Ferroelectr., Freq. Control*, vol. 54, no. 2, pp. 251–270, Feb. 2007.

[3] M. Rinaldi, C. Zuniga, C. Zuo, and G. Piazza, "Super-high-frequency two-port AlN contour-mode resonators for RF applications," *IEEE Trans. Ultrason., Ferroelectr., Freq. Control*, vol. 57, no. 1, pp. 38–45, Jan. 2010.

[4] A. Hajjam, J. C. Wilson, A. Rahafrooz, and S. Pourkamali, "Fabrication and characterization of thermally actuated micromechanical resonators for airborne particle mass sensing—Part II: Device fabrication and characterization," *J. Micromech. Microeng.*, vol. 20, no. 12, p. 125 019, Dec. 2010.

[5] A. Hajjam, J. C. Wilson, and S. Pourkamali, "Individual air-borne particle mass measurement using high frequency micromechanical resonators," *IEEE Sens. J.*, vol. 11, no. 11, pp. 2883–2890, Nov. 2011.

[6] R. Melamud, S. A. Chandorkar, K. Bongsang, K. L. Hyung, J. C. Salvia, G. Bahl, M. A. Hopcroft, and T. W. Kenny, "Temperature-insensitive composite micromechanical resonators," *J. Microelectromech. Syst.*, vol. 18, no. 6, pp. 1409–1419, Dec. 2009.

[7] S. Pourkamali, K. Ho, and F. Ayazi, "Low-impedance VHF and UHF capacitive SiBARs—Part I: Concept and fabrication," *IEEE Trans. Electron Devices*, vol. 54, no. 8, pp. 2017–2023, Aug. 2007.

[8] Product data sheet, SMD2520 Crystal, Fronter Electronics. [Online]. Available: http://www.chinafronter.com/PIC/PIC/201051112480.pdf

[9] Oscilent Product data sheet, 500 series temperature compensated crystal oscillators (TCXO). [Online]. Available: http://www.oscilent.com/catalog/Category/TCXO_VCXO_VCO.html

[10] K. Sundaresan, G. K. Ho, S. Pourkamali, and F. Ayazi, "Electronically temperature compensated silicon bulk acoustic resonator reference oscillator," *IEEE J. Solid-State Circuits*, vol. 42, no. 6, pp. 1425–1434, Jun. 2007.

[11] J. C. Salvia, R. Melamud, S. A. Chandorkar, S. F. Lord, and T. W. Kenny, "Real-time temperature compensation of MEMS oscillators using an integrated micro-oven and a phase-locked loop," *J. Microelectromech. Syst.*, vol. 19, no. 1, pp. 192–201, Feb. 2010.

[12] C. T.-C. Nguyen and R. T. Howe, "Micro-resonator frequency control and stabilization using an integrated micro oven," in *Proc. IEEE Transducers Conf.*, Boston, MA, Jun. 1993, pp. 1040–1043.

[13] C. M. Jha, M. A. Hopcroft, S. A. Chandorkar, J. C. Salvia, M. Agarwal, R. N. Candler, R. Melamud, K. Bongsang, and T. W. Kenny, "Thermal isolation of encapsulated MEMS resonators," *J. Microelectromech. Syst.*, vol. 17, no. 1, pp. 175–184, Feb. 2008.

[14] W.-T. Hsu and C. T.-C. Nguyen, "Stiffness compensated temperature insensitive micromechanical resonators," in *Proc. IEEE MEMS*, Las Vegas, NV, Jan. 2002, pp. 731–734.

[15] R. Tabrizian, G. Casinovi, and F. Ayazi, "Temperature-stable high-Q AlN-on-silicon resonators with embedded array of oxide pillars," in *Proc. Hilton Head Solid-State Sens., Actuators, Microsyst. Workshop*, Jun. 2010, pp. 100–101.

[16] J. S. Wang and K. M. Lakin, "Low-temperature coefficient bulk acoustic wave composite resonators," *Appl. Phys. Lett.*, vol. 40, no. 4, pp. 308–310, Feb. 1982.

[17] A. K. Samarao, G. Casinovi, and F. Ayazi, "Passive TCF compensation in high Q silicon micromechanical resonators," in *Proc. IEEE MEMS*, Hong Kong, Jan. 2010, pp. 116–119.

[18] A. K. Samarao and F. Ayazi, "Temperature compensation of silicon micromechanical resonators via degenerate doping," in *IEDM Tech. Dig.*, Dec. 2009, pp. 1–4.

[19] A. Rahafrooz, A. Hajjam, B. Tousifar, and S. Pourkamali, "Thermal actuation, a suitable mechanism for high frequency electromechanical resonators," in *Proc. IEEE MEMS*, Jan. 2010, pp. 200–203.

[20] A. Hajjam and S. Pourkamali, "Fabrication and characterization of MEMS-based resonant organic gas sensors," *IEEE Sens. J.*, to be published.

[21] A. Hajjam, A. Rahafrooz, and S. Pourkamali, "Sub-100 ppb/°C temperature stability in thermally actuated high frequency silicon resonators via degenerate phosphorous doping and bias current optimization," in *IEDM Tech. Dig.*, Dec. 2010, pp. 7.5.1–7.5.4.

[22] A. Hajjam, A. Rahafrooz, and S. Pourkamali, "Temperature compensated single-device electromechanical oscillators," in *Proc. IEEE MEMS*, Jan. 2011, pp. 801–804.

[23] G. K. Ho, K. Sundaresan, S. Pourkamali, and F. Ayazi, "Micromechanical IBARs: Tunable high-Q resonators for temperature-compensated reference oscillators," *J. Microelectromech. Syst.*, vol. 19, no. 3, pp. 503–515, Jun. 2010.

[24] S. Veprek, "Electronic and mechanical properties of nanocrystalline composites when approaching molecular size," *J. Thin Solid Films*, vol. 297, no. 1/2, pp. 145–153, Apr. 1997.

Arash Hajjam (S'09) was born in Tehran, Iran. He received the B.S. degree in electrical engineering from the University of Tehran, Tehran, in 2005, and the M.S. degree in bioelectrical engineering from Iran University of Science and Technology, Tehran, in 2008. He is currently working toward the Ph.D. degree in the Department of Electrical and Computer Engineering, University of Denver, Denver, CO.

His research interests include microelectromechanical system frequency references and resonant sensors.

Mr. Hajjam is a Licensed Professional Engineer in the State of Colorado. He received the Best Teaching Assistant Award from the School of Engineering and Computer Science, University of Denver, in 2009 and was the recipient of the Best Student Paper Award at the 2004 ISCEE Electrical Engineering Conference.

Andrew Logan was born in Littleton, CO. He is currently working toward the Bachelor's degree in electrical engineering, with a focus on power systems, at the University of Southern California, Los Angeles.

His interest in research began in college when he started taking engineering courses. He was offered a position as a Research Assistant under Dr. S. Pourkamali for being at the top of his class. His research interests include MEMS and NEMS, robotics, optics, and power systems.

Siavash Pourkamali (S'02–M'06) received the B.S. degree in electrical engineering from Sharif University of Technology, Tehran, Iran, in 2001, and the M.S. and Ph.D. degrees in electrical engineering from Georgia Institute of Technology, Atlanta, in 2004 and 2006, respectively.

He is currently an Assistant Professor in the Department of Electrical and Computer Engineering, University of Denver, Denver, CO. He is the holder of several issued patents and pending patent applications in the areas of silicon micro/nanomechanical resonators and filters and nanofabrication technologies, some of which have been licensed to major players in the semiconductor industry. His main research interests include the areas of integrated silicon-based MEMS and microsystems, micromachining technologies, RF MEMS resonators and filters, and nanomechanical resonant sensors.

Dr. Pourkamali was a recipient of a 2011 National Science Foundation CAREER Award, the 2008 University of Denver Best Junior Scholar Award, and the 2006 Georgia Tech Electrical and Computer Engineering Research Excellence Award. He was also a silver medalist in the 29th International Chemistry Olympiad (ICHO) in 1997.